

EarthArXiv Coversheet

Robert Kostynick¹, Julia Prata¹, Jesse Bower², and Claire Masteller¹

¹Earth, Environmental, and Planetary Sciences, Washington University in St. Louis, St. Louis, MO, USA

²Department of Civil & Environmental Engineering, Utah State University, Logan, UT, USA

cmasteller@wustl.edu

This pre-print is in review at *Geology* and has undergone no rounds of peer-review.

1 Slope-dependent riverbed strengthening and the evolution of the
2 threshold for motion in gravel-bed rivers

3 **Robert Kostynick¹, Julia Prata¹, Jesse Bower², and Claire Masteller¹**

4 *¹Department of Earth, Environmental, and Planetary Sciences, Washington University in St.
5 Louis, St. Louis, MO, USA*

6 *²Department of Civil and Environmental Engineering, Utah State University, Logan, UT, USA*

7 **ABSTRACT**

8 The threshold for motion exerts a fundamental control on sediment transport, channel
9 morphology, and fluvial erosion. While channel slope and flow history are known to influence
10 entrainment thresholds in gravel-bed rivers, their interaction has not been explored. We
11 investigate how channel slope modulates riverbed strengthening during low-flow periods. Flume
12 experiments were conducted across slopes spanning more than an order of magnitude ($S=5-70$
13 mm/m) with hydraulic forcing scaled relative to slope-specific entrainment thresholds. Across all
14 slopes, sediment flux decreased with increasing conditioning time, indicating progressive
15 riverbed strengthening. Strengthening rates increased strongly with slope, reflecting more
16 effective stabilization by low flows. At steep slopes, reduced hydrodynamic lift forces may
17 combine with ongoing granular rearrangement during low flows to progressively stabilize the
18 bed, increasing grain resistance to entrainment. These results demonstrate that slope exerts a
19 strong control on riverbed recovery following floods. Because strengthening rates scale
20 predictably with channel gradient, slope may provide a first-order parameter for predicting flow-
21 history-driven evolution of entrainment thresholds in sediment transport models, with

22 implications for erosion rates, channel form, and the distribution of geomorphic work across
23 watersheds.

24

25 **INTRODUCTION**

26 River erosion shapes landscapes by carving valleys (Brocard and van der Beek, 2006),
27 organizing drainage networks (Gasparini et al., 2004), and regulating the delivery of water and
28 sediment to oceans (Syvitski et al., 2005). In gravel-bed rivers, sediment transport controls both
29 the pace of erosion and channel morphology (Parker, 1978; Phillips et al., 2022), influencing
30 flood hazards, aquatic habitat structure, and water quality. Despite the central role of sediment
31 transport in shaping rivers and landscapes, accurate predictions of bedload flux remain
32 challenging due to the complex coupling between turbulent flow and granular riverbeds
33 (Jerolmack and Daniels, 2019; Hosseiny et al., 2023). Addressing this challenge requires a
34 deeper understanding of the physical processes that govern how rivers erode their beds.

35 A fundamental control on sediment transport and fluvial erosion is the threshold for
36 sediment motion, which defines the flow conditions above which rivers can mobilize the
37 riverbed. When flows exceed this threshold, bedload transport conveys sediment downstream.
38 This redistribution of sediment along river channels can, in turn, alter channel morphology.
39 Further, once the entrainment threshold is exceeded, sediment transport intensity and grain
40 impact energies increase rapidly, influencing bedrock erosional efficiency (Sklar and Dietrich,
41 2004; Masteller et al., 2024). In this way, the threshold for motion controls which floods are
42 most effectively translated into geomorphic work, governing the portion of the discharge
43 distribution that contributes to landscape change (DiBiase and Whipple, 2011). The threshold for
44 motion also underpins channel geometry such that rivers adjust their width, depth, and slope so

45 that at bankfull conditions, flows only slightly exceed the threshold for motion, allowing
46 sediment to be transported downstream without significant bank erosion (Parker, 1978; Phillips
47 et al., 2022).

48 The threshold for motion is commonly represented as critical Shields stress, τ_c^* , a
49 nondimensional parameter normalizing boundary shear stress by sediment grain size (Shields,
50 1936). In many applications, critical Shields stress is held constant, with bedload flux formulae
51 often assuming a specific value of τ_c^* (e.g. Wong and Parker, 2006). Early data compilations
52 suggested that τ_c^* occupies a narrow range (0.03–0.1; e.g., Buffington and Montgomery, 1997).
53 However, subsequent work has shown that the threshold for motion can vary widely across rivers
54 and through time. This variability arises from changes in hydraulic conditions (Lamb et al.,
55 2017), riverbed structure (Kirchner et al., 1990; Whitfield et al., 2025), sediment supply (Yager
56 et al., 2012; Johnson, 2016), grain exposure and protrusion (Masteller and Finnegan, 2017;
57 Yager et al., 2018; Hodge et al., 2019), and even biological activity (Albertson et al., 2014;
58 Masteller et al., 2015).

59 Channel slope exerts a strong control on entrainment thresholds. Steeper slopes produce
60 shallower flows and greater relative roughness, modifying turbulent structures and grain-scale
61 forces acting on the bed (Mueller et al., 2005; Lamb et al., 2008, 2017; Prancevic and Lamb,
62 2015). As a result, τ_c^* systematically increases with channel slope despite greater downstream
63 gravitational forcing. Masteller et al. (in review) highlights that this relationship is reflected in
64 bankfull channel geometry within individual river systems, with steep headwaters organizing to
65 reflect higher bankfull Shields stresses relative to low-slope downstream reaches.

66 Riverbed erosion thresholds also evolve through time. Numerous studies have
67 demonstrated that τ_c^* is sensitive to the history of recent flows, reflecting a “memory” of the

68 magnitude and duration of previous hydraulic forcing. Periods of low flow allow grains to
69 rearrange locally, reducing protrusion and increasing τ_c^* between transport events (Ockelford and
70 Haynes, 2013; Masteller and Finnegan, 2017). Subsequent high-magnitude floods can disrupt
71 this strengthened bed structure by mobilizing grains and resetting τ_c^* (Turowski et al., 2009;
72 Masteller et al., 2019). Building on these observations, Masteller et al. (2025) developed a model
73 that captures the temporal evolution of τ_c^* by weighting the competing effects of riverbed
74 strengthening and weakening as a function of flow history. These history-dependent thresholds
75 are also expressed in channel geometry, with rivers experiencing lower bankfull intermittency
76 tending to be narrower than those with high intermittency (Phillips et al., 2024).

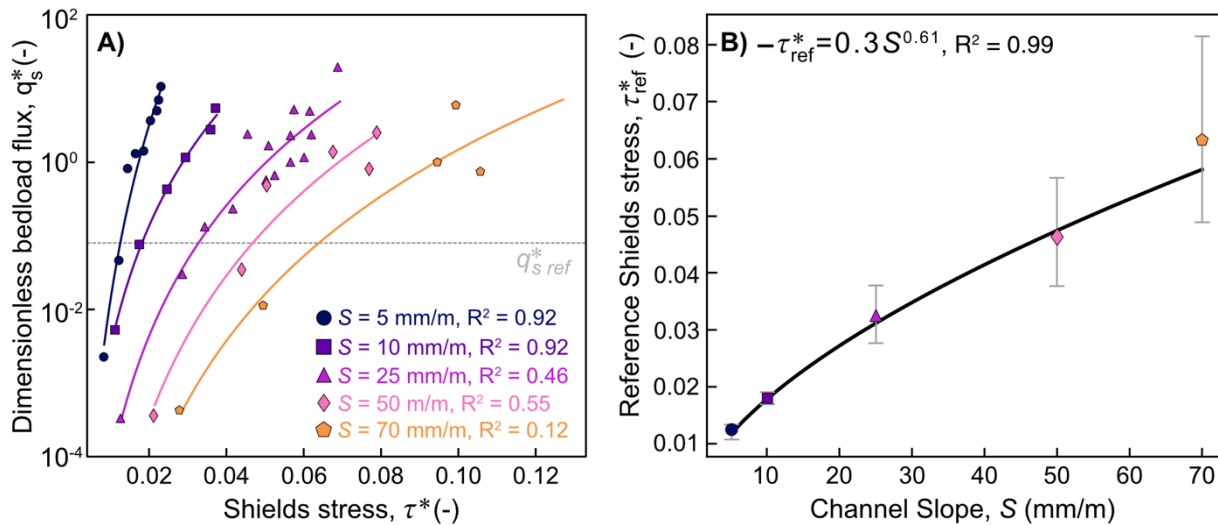
77 Although both slope and flow history exert strong influences on τ_c^* , how these effects
78 interact has never been directly explored. As a result, we lack a mechanistic understanding of
79 how channel slope influences the rate and magnitude of riverbed strengthening during low flows.
80 This knowledge gap limits our ability to predict how sediment transport thresholds and by
81 extension, river morphology, varies along river networks.

82 **EXPERIMENTAL DESIGN AND HYDRAULIC SCALING**

83 To investigate how channel slope influences riverbed strengthening during low flows, we
84 conducted a series of flume experiments in a 0.4 m wide, 4.5 m long tilting flume. The upstream
85 end of the flume is mounted on hydraulic cylinders that allow the flume to be adjusted over a
86 wide range of slopes. We completed experiments at four slopes spanning over an order of
87 magnitude: $S=5, 25, 50, \text{ and } 70$ mm/m. The channel bed consisted of a gravel mixture with
88 median grain size $D_{50}=7.4$ mm and a lognormal grain-size distribution, selected to approximate
89 natural gravel-bed rivers and facilitate comparison with previous experiments (Masteller and

90 Finnegan, 2017). Sediment exiting the flume was captured in a downstream basket to quantify
 91 bedload transport rates.

92 To ensure that all runs experienced equivalent flow histories despite large differences in
 93 channel slope, hydraulic forcing was scaled relative to τ_c^* specific to each slope, rather than
 94 applying identical discharges or Shields stresses across experiments. Sediment transport rating
 95 curves were constructed from a series of short (3 min) transport runs spanning a range of flow
 96 depths (Fig. 1A). Slope-specific reference Shields stress, τ_{ref}^* , was then estimated from each
 97 rating curves using a reference dimensionless transport rate, $q_s^* = 0.08$ (e.g. Prancevic and Lamb,
 98 2015; Fig. 2B). τ_{ref}^* increases systematically with channel slope, ranging from $\tau_{ref}^* = 0.012$ to
 99 0.063, and is well described by $\tau_{ref}^* = 0.30S^{0.61}$ ($R^2 = 0.99$).



100

101 **Figure 1.** A) sediment transport rating curves; B) Estimates of τ_{ref}^* with channel slope; error
 102 bars represent the 75% confidence interval.

103 For each slope, low-flow conditioning and above-threshold transport flows were
 104 prescribed as fixed fractions of τ_{ref}^* , with conditioning flows targeting $0.75\tau_{ref}^*$ and transport
 105 floods, $1.2\tau_{ref}^*$. By scaling conditioning and transport flows, experiments conducted at different

106 slopes experienced near identical flow histories relative to their slope-specific entrainment
107 thresholds, allowing for direct comparison.

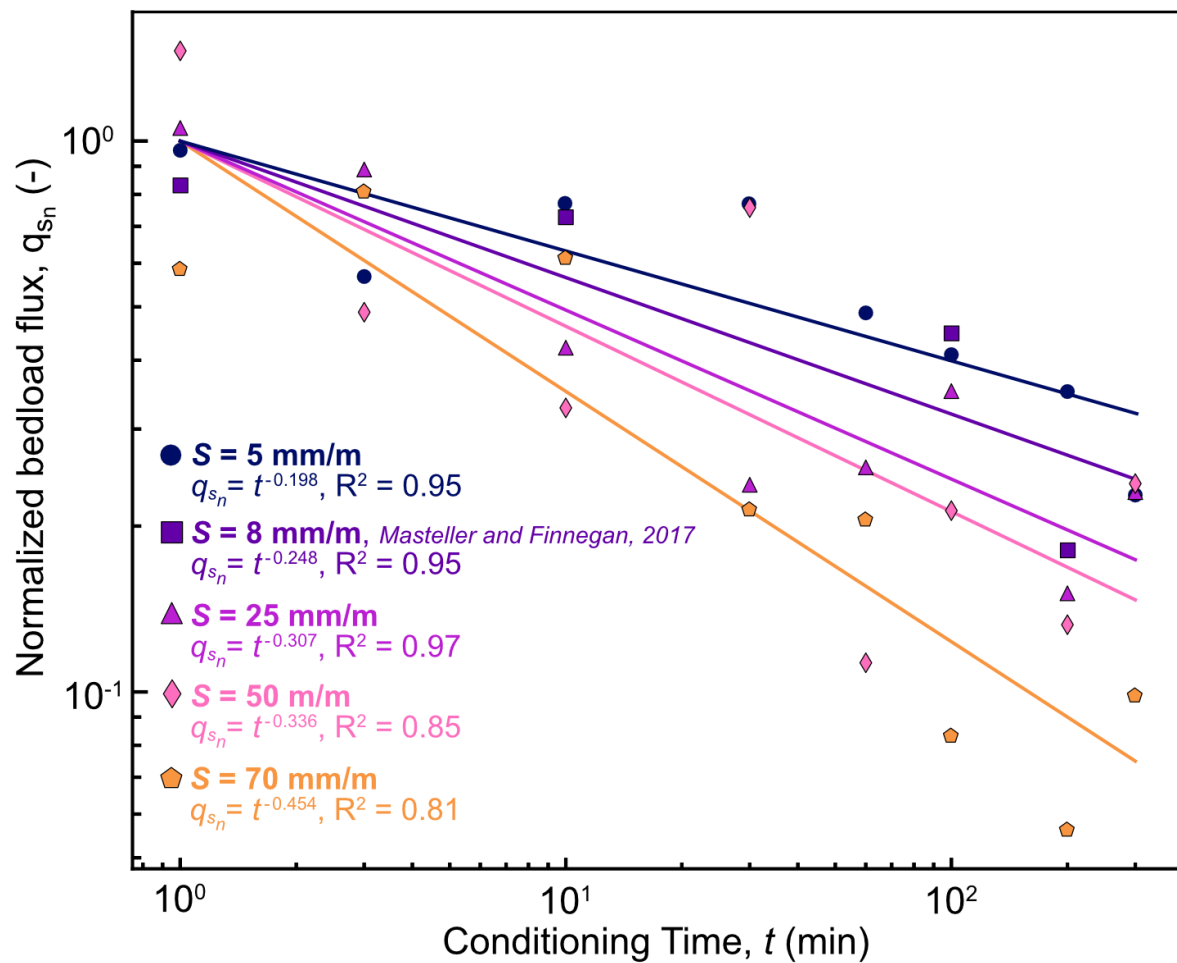
108 Each experiment had three stages designed to isolate the effects of antecedent low flows
109 on sediment mobility. First, the bed was manually mixed, screeded, and leveled to remove any
110 armoring and bed structure, ensuring the most reproducible initial condition possible. The bed
111 was then subjected to a conditioning flow ($0.75\tau_{ref}^*$) lasting between 1 and 300 minutes.
112 Following conditioning, a short-duration transport flood (5 min) was applied to mobilize
113 sediment and drive bedload transport. For shorter conditioning times where transport rates were
114 more variable, replicate runs were performed and median sediment flux is reported.

115 **SLOPE-DEPENDENT RIVERBED STRENGTHENING**

116 Sediment flux, q_s (kg/m/s), following the transport flood decreases systematically with
117 increasing conditioning time across all experimental slopes with significant negative correlations
118 (Spearman's ρ : -0.71 to -0.88, all p-values < 0.047). Across all experimental slopes, longer
119 antecedent low flows produce progressively lower bedload transport rates. After 300 minutes of
120 conditioning, average bedload flux decreases by a factor of 4 at the lowest slopes and to over an
121 order of magnitude at the steepest slopes. Reductions in flux are most rapid in early stages of
122 conditioning, with transport rates plateauing at minimum values for low flows exceeding 100
123 minutes.

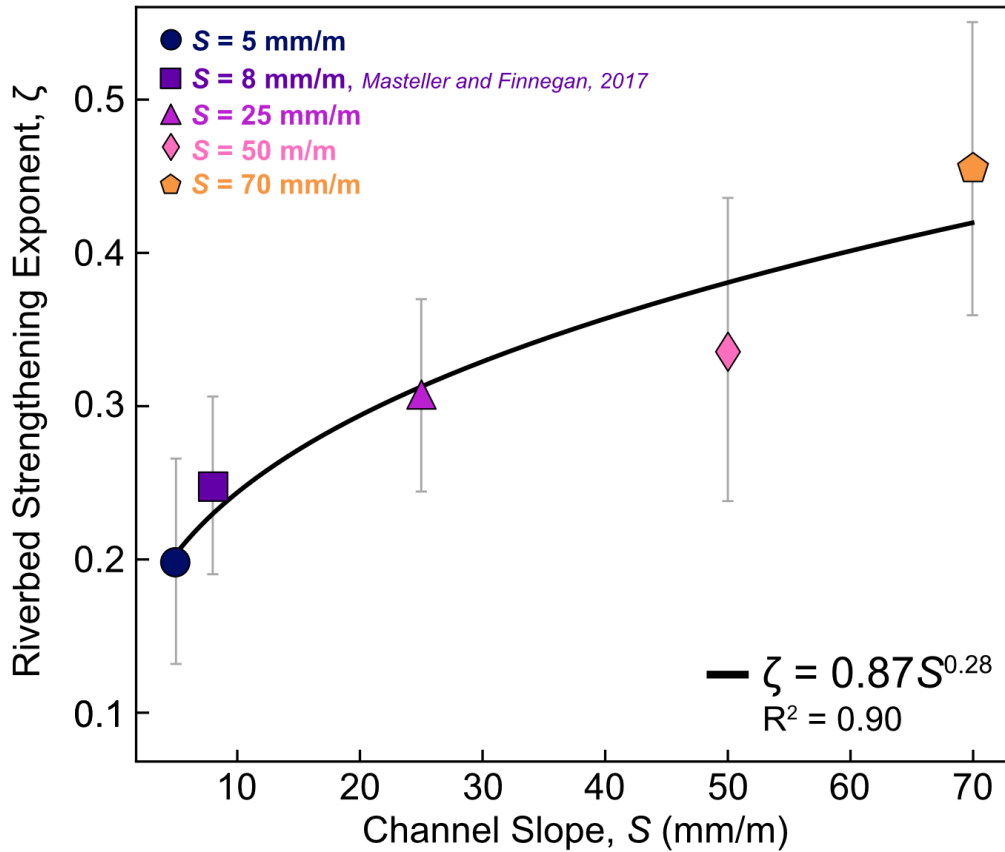
124 To quantify the rate of riverbed strengthening, we fit a power-law to each slope-specific
125 dataset of the form $q_s = \alpha t^{-\zeta}$, where t is low flow conditioning time and ζ is the riverbed
126 strengthening exponent. Larger values of ζ reflect more efficient strengthening. To facilitate
127 comparison across slopes and with previous experiments from Masteller and Finnegan (2017)
128 ($S=8$ mm/m), q_s was normalized using the data-derived α values for each slope set to account for

129 differences in initial bed conditions and uncertainties in threshold estimates (Fig. 2). This
 130 normalization affects only the coefficient of the flux-time relationship and does not influence the
 131 value of ζ or the goodness-of-fit with conditioning time. Across experiments, flux is well
 132 described by power-law fits with $R^2=0.81-0.97$. Goodness-of-fit metrics are reduced for steep
 133 slopes, where shallow flows introduce greater uncertainty in estimates of Shields stress and
 134 experimental scaling.



135
 136 **Figure 2.** Normalized sediment flux, q_{sn} , with conditioning time for each experimental slope and
 137 data from Masteller and Finnegan (2017) with best-fit power laws.
 138

139 ζ increases systematically with slope, indicating that riverbeds strengthen more rapidly at
140 steeper slopes (Fig. 3). For the lowest slope $S=5$ mm/m, $\zeta=0.149$ ($R^2=0.93$), compared to a
141 $\zeta=0.454$ ($R^2=0.81$) at $S=70$ mm/m. These differences in ζ imply large contrasts in the degree of
142 transport reduction across our experiments. Over 300 minutes of conditioning, ζ predicts only a
143 ~ 2 -fold reduction in flux at $S=0.005$, whereas the highest-slope ζ predicts over an order-of-
144 magnitude (~ 13 -fold) reduction. These results highlight that even under near identical flow
145 histories, riverbeds at steeper slopes stabilize far more efficiently during low flow. Indeed, ζ
146 scales systematically with channel slope following a power-law relationship, $\zeta = 0.87S^{0.28}$
147 ($R^2=0.90$; Fig. 3). Strengthening exponents derived from previously published experiments
148 conducted in a different flume (Masteller and Finnegan, 2017) fall directly along the trend
149 defined by our experimental data. The remarkably strong fit of this relationship indicates that the
150 rate at which riverbeds strengthen during low flows varies systematically and predictably with
151 channel slope.



152

153 **Figure 3.** Riverbed strengthening exponent, ζ , as a function of slope. Error bars denote ± 1
 154 standard deviation uncertainty associated with the power-law fits used to estimate ζ .

155

156 **IMPLICATIONS FOR RIVER PROCESS AND FORM**

157 Our experiments provide the first demonstration that channel slope has a strong influence
 158 on flow-history-driven evolution of entrainment thresholds. Although riverbed strengthening
 159 during low flow has been documented in laboratory and field studies (e.g., Masteller and
 160 Finnegan, 2017; Masteller et al., 2019), our results demonstrate that strengthening rate varies
 161 systematically with channel slope. Riverbeds at steeper slopes stabilize more rapidly during low
 162 flows, even when hydraulic forcing is scaled relative to slope-specific entrainment thresholds.
 163 The strengthening exponent, ζ , varies predictably with slope, suggesting that channel gradient

164 governs the rate at which riverbeds recover stability after floods by influencing the physical
165 processes that stabilize the bed surface. This finding is particularly significant because it implies
166 that models describing the evolution of τ_c^* as a function of flow history (e.g., Masteller et al.,
167 2025) may be parameterized across river networks using channel slope as a predictor of relative
168 strengthening rates.

169 Sediment flux in gravel-bed rivers is often strongly influenced by the most highly
170 protruding grains on the bed surface, which are preferentially exposed to hydrodynamic forces
171 and therefore more susceptible to entrainment (Yager et al., 2018; Hodge et al., 2019). Previous
172 work has also shown that the number of protruding grains can decrease during periods of low-
173 flow conditioning as grains reorganize into more stable configurations (Masteller and Finnegan,
174 2017). These observations suggest that protrusion may provide an important grain-scale control
175 on how riverbeds strengthen between floods. However, more work is needed to determine
176 whether the same population of highly protruding grains governs sediment transport across all
177 channel slopes, or if effective protrusion thresholds that influence mobility shift with channel
178 gradient.

179 One possible mechanism for enhanced strengthening at steep slopes involves the
180 interaction of grain-scale rearrangement and shallow-flow hydraulics. Lower relative
181 submergence, or the ratio of flow depth to grain size, increases grain exposure to flow,
182 strengthening the interaction between sediment grains and turbulent fluctuations. During low-
183 flow conditioning, near-threshold stresses acting on exposed grains, paired with a greater
184 downslope gravitational force, may more effectively pivot grains into pockets and more stable
185 configurations. During floods, shallow-flow hydraulics may further enhance bed stability. At
186 steep slopes, flow depths approach grain-scale roughness heights ($h/D_{50} \lesssim 1$) and turbulent wakes

187 around grains can reduce or even reverse lift forces (Lamb et al., 2017). Under these conditions,
188 high protruding grains become more difficult to dislodge. Together, these processes may
189 combine to cause riverbeds at steeper slopes stabilize more efficiently in response to the same
190 flow history.

191 Sediment entrainment at steep slopes may also become increasingly controlled by
192 intermittent turbulence or particle collisions. If beds at steep slopes are more stable overall,
193 grains may remain immobile under typical boundary shear stresses and only become mobilized
194 primarily during brief, high-magnitude fluctuations in flow. Turbulent sweeps and bursts can
195 generate large instantaneous forces capable of entraining grains that would otherwise remain
196 stable (e.g., Diplas et al., 2008). Under such conditions, sediment transport may become
197 dominated by rare stochastic events rather than sustained hydraulic forcing, potentially allowing
198 grains across a broader range of protrusions to contribute to sediment flux. Alternatively,
199 collisions may drive collective entrainment (e.g. Lee and Jerolmack, 2018), where impacts
200 mobilize neighboring particles largely independent of their protrusion. Greater overall bed
201 stability at steep slopes may therefore shift sediment transport toward rare, stochastic events
202 rather than sustained forcing acting on the most exposed grains.

203 **CONCLUSIONS**

204 Our results show that slope exerts a previously unrecognized control on riverbed
205 resilience and recovery following disturbance by floods. If steep channels recover bed stability
206 more rapidly during intervening low-flow periods, their beds spend a greater fraction of time in a
207 strengthened state characterized by elevated τ_c^* . This could systematically alter how geomorphic
208 work is distributed across rivers, shifting the floods that accomplish the most sediment transport
209 and bedrock erosion toward larger, less frequent events in steep channel headwaters. Such shifts

210 may drive headwater reaches to organize around bankfull geometries that reflect elevated τ_c^* and
211 longer bankfull recurrence intervals. Patterns consistent with this idea have been observed in
212 mountain rivers, where bankfull channel morphology in headwaters indicates reduced mobility
213 relative to low-gradient downstream reaches (Mueller et al., 2005; Masteller et al.). As such, the
214 joint impact of channel slope and flow-history on τ_c^* may give rise to distinct, catchment-specific
215 scaling relationships in bankfull hydraulic geometry across river networks (Kostynick et al.,
216 2026). Additional work is needed to disentangle transient strengthening effect from the broader
217 influence of slope on sediment entrainment thresholds and stable channel form. Our results
218 reveal that channel gradient regulates how rivers retain and express the memory of past flows
219 through evolving entrainment thresholds. Incorporating slope-dependent flow-history-effects into
220 sediment transport and incision models can help to improve predictions of how river networks
221 respond to and integrate hydroclimatic variability.

222

223 **ACKNOWLEDGMENTS**

224 Research was supported by the NSF Division of Earth Sciences EAR-2220504 and EAR-
225 2220505.

226

227 **REFERENCES CITED**

228 Albertson, L.K., Sklar, L.S., Pontau, P., Dow, M., and Cardinale, B.J., 2014, A mechanistic
229 model linking insect (Hydropsychidae) silk nets to incipient sediment motion in gravel-
230 bedded streams: *Journal of Geophysical Research: Earth Surface*, v. 119, p. 1833–1852,
231 doi:10.1002/2013JF003024.

232 Brocard, G.Y., and van der Beek, P.A., 2006, Influence of incision rate, rock strength, and
233 bedload supply on bedrock river gradients and valley-flat widths: Field-based evidence
234 and calibrations from western Alpine rivers (southeast France), *in* *Tectonics, Climate,*
235 *and Landscape Evolution*, Geological Society of America, doi:10.1130/2006.2398(07).

- 236 Buffington, J.M., and Montgomery, D.R., 1997, A systematic analysis of eight decades of
237 incipient motion studies, with special reference to gravel-bedded rivers: *Water Resources*
238 *Research*, v. 33, p. 1993–2029, doi:<https://doi.org/10.1029/96WR03190>.
- 239 DiBiase, R.A., and Whipple, K.X., 2011, The influence of erosion thresholds and runoff
240 variability on the relationships among topography, climate, and erosion rate: *Journal of*
241 *Geophysical Research*, 116(F4), F04036.
- 242 Gasparini, N.M., Tucker, G.E., and Bras, R.L., 2004, Network-scale dynamics of grain-size
243 sorting: implications for downstream fining, stream-profile concavity, and drainage basin
244 morphology: *Earth Surface Processes and Landforms*, v. 29, p. 401–421,
245 doi:[10.1002/esp.1031](https://doi.org/10.1002/esp.1031).
- 246 Hodge, R.A., Voepel, H., Leyland, J., Sear, D.A., and Ahmed, S., 2019, X-ray computed
247 tomography reveals that grain protrusion controls critical shear stress for entrainment of
248 fluvial gravels: *Geology*, v. 48, p. 149–153, doi:[10.1130/G46883.1](https://doi.org/10.1130/G46883.1).
- 249 Hosseiny, H., Masteller, C.C., Dale, J.E., and Phillips, C.B., 2023, Development of a machine
250 learning model for river bed load: *Earth Surface Dynamics*, v. 11, p. 681–693,
251 doi:[10.5194/esurf-11-681-2023](https://doi.org/10.5194/esurf-11-681-2023).
- 252 Jerolmack, D.J., and Daniels, K.E., 2019, Viewing Earth’s surface as a soft-matter landscape:
253 *Nature Reviews Physics*, v. 1, p. 716–730, doi:[10.1038/s42254-019-0111-x](https://doi.org/10.1038/s42254-019-0111-x).
- 254 Johnson, J.P.L., 2016, Gravel threshold of motion: a state function of sediment transport
255 disequilibrium? *Earth Surface Dynamics*, v. 4, p. 685–703, doi:[10.5194/esurf-4-685-](https://doi.org/10.5194/esurf-4-685-2016)
256 [2016](https://doi.org/10.5194/esurf-4-685-2016).
- 257 Kirchner, J.W., Dietrich, W.E., Iseya, F., and Ikeda, H., 1990, The variability of critical shear
258 stress, friction angle, and grain protrusion in water-worked sediments: *Sedimentology*, v.
259 37.
- 260 Kostynick, R.P., Phillips, C.B., and Masteller, C.C., 2026, High-Resolution Channel Geometry
261 Reveals Contrasting Styles of Gravel River Adjustment: *Geophysical Research Letters*,
262 doi:[10.1029/2025GL118412](https://doi.org/10.1029/2025GL118412).
- 263 Lamb, M.P., Brun, F., and Fuller, B.M., 2017, Direct measurements of lift and drag on shallowly
264 submerged cobbles in steep streams: Implications for flow resistance and sediment
265 transport: *Water Resources Research*, v. 53, p. 7607–7629, doi:[10.1002/2017WR020883](https://doi.org/10.1002/2017WR020883).
- 266 Lamb, M.P., Dietrich, W.E., and Venditti, J.G., 2008, Is the critical Shields stress for incipient
267 sediment motion dependent on channel-bed slope? *Journal of Geophysical Research*, v.
268 113, p. F02008, doi:[10.1029/2007JF000831](https://doi.org/10.1029/2007JF000831).
- 269 Lee, D.B., and Jerolmack, D., 2018, Determining the scales of collective entrainment in
270 collision-driven bed load: *Earth Surface Dynamics*, v. 6.

- 271 Masteller, C.C., Chandler, H., and Bower, J., 2024, The Fluvial Battering Ram: Collisional
272 Experiments Reveal the Importance of Particle Impact Energies on Bedrock Erosional
273 Efficiency: *Geophysical Research Letters*, v. 51, p. e2024GL109533,
274 doi:10.1029/2024GL109533.
- 275 Masteller, C.C., and Finnegan, N.J., 2017, Interplay between grain protrusion and sediment
276 entrainment in an experimental flume: *Journal of Geophysical Research: Earth Surface*,
277 v. 122, p. 274–289, doi:10.1002/2016JF003943.
- 278 Masteller, C.C., Finnegan, N.J., Turowski, J.M., Yager, E.M., and Rickenmann, D., 2019,
279 History-Dependent Threshold for Motion Revealed by Continuous Bedload Transport
280 Measurements in a Steep Mountain Stream: *Geophysical Research Letters*, v. 46.
- 281 Masteller, C.C., Finnegan, N.J., Warrick, J.A., and Miller, I.M., 2015, Kelp, cobbles, and
282 currents: Biologic reduction of coarse grain entrainment stress: *Geology*, v. 43, p. 543–
283 546, doi:10.1130/G36616.1.
- 284 Masteller, C.C., Johnson, J.P.L., Rickenmann, D., and Turowski, J.M., 2025, Modeling memory
285 in gravel-bed rivers: a flow-history-dependent relation for evolving thresholds of motion:
286 *Earth Surface Dynamics*, v. 13, p. 593–605, doi:10.5194/esurf-13-593-2025.
- 287 Masteller, C.C., Phillips, C.B., Kostynick, R.P., Castejon-Villalobos, J.F., Lopez, C.G., Shallue,
288 M.K., Bower, J., and Sigman, A. Tracking the trajectory of alluvial channel adjustment
289 along a river's profile.: [https://www.authorea.com/users/721760/articles/1389848-](https://www.authorea.com/users/721760/articles/1389848-tracking-the-trajectory-of-alluvial-channel-adjustment-along-a-river-s-profile?commit=6b8c3cfa541fa066011c7bd093ab3cbce4fe7c62)
290 [tracking-the-trajectory-of-alluvial-channel-adjustment-along-a-river-s-](https://www.authorea.com/users/721760/articles/1389848-tracking-the-trajectory-of-alluvial-channel-adjustment-along-a-river-s-profile?commit=6b8c3cfa541fa066011c7bd093ab3cbce4fe7c62)
291 [profile?commit=6b8c3cfa541fa066011c7bd093ab3cbce4fe7c62](https://www.authorea.com/users/721760/articles/1389848-tracking-the-trajectory-of-alluvial-channel-adjustment-along-a-river-s-profile?commit=6b8c3cfa541fa066011c7bd093ab3cbce4fe7c62) (accessed March 2026).
- 292 Mueller, E.R., Pitlick, J., and Nelson, J.M., 2005, Variation in the reference Shields stress for
293 bed load transport in gravel-bed streams and rivers: *Water Resources Research*, v. 41, p.
294 W04006, doi:10.1029/2004WR003692.
- 295 Ockelford, A.-M., and Haynes, H., 2013, The impact of stress history on bed structure: *Earth*
296 *Surface Processes and Landforms*, v. 38, p. 717–727,
297 doi:<https://doi.org/10.1002/esp.3348>.
- 298 Parker, G., 1978, Self-formed straight rivers with equilibrium banks and mobile bed. Part 2: The
299 gravel river. *Journal of Fluid Mechanics*, v. 89, p. 127–146,
300 doi:10.1017/S0022112078002505.
- 301 Phillips, C.B., Masteller, C.C., Blaylock, J., Van Iwaarden, F., and Johnson, J.P.L., 2024,
302 Variability in River Width Reveals Climatic Influence on Channel Geometry:
303 *Geophysical Research Letters*, v. 51, p. e2024GL111789, doi:10.1029/2024GL111789.
- 304 Phillips, C.B., Masteller, C.C., Slater, L.J., Dunne, K.B.J., Francalanci, S., and Lanzoni, S.,
305 2022, Threshold constraints on the size, shape and stability of alluvial rivers: *Nature*
306 *Reviews Earth & Environment*, p. 1–14, doi:10.1038/s43017-022-00282-z.

- 307 Prancevic, J.P., and Lamb, M.P., 2015, Unraveling bed slope from relative roughness in initial
308 sediment motion: Relative roughness and incipient motion: Journal of Geophysical
309 Research: Earth Surface, v. 120, p. 474–489, doi:10.1002/2014JF003323.
- 310 Shields, A., 1936, Application of similarity principles and turbulence research to bed-load
311 movement., <https://resolver.caltech.edu/CaltechKHR:HydroLabpub167> (accessed
312 January 2021).
- 313 Sklar, L.S., and Dietrich, W.E., 2004, A mechanistic model for river incision into bedrock by
314 saltating bed load: Water Resources Research, v. 40, doi:10.1029/2003WR002496.
- 315 Syvitski, J.P.M., Vörösmarty, C.J., Kettner, A.J., and Green, P., 2005, Impact of humans on the
316 flux of terrestrial sediment to the global coastal ocean: Science, v. 308, p. 376–380,
317 doi:10.1126/science.1109454.
- 318 Turowski, J.M., Yager, E.M., Badoux, A., Rickenmann, D., and Molnar, P., 2009, The impact of
319 exceptional events on erosion, bedload transport and channel stability in a step-pool
320 channel: Earth Surface Processes and Landforms, v. 34, p. 1661–1673,
321 doi:10.1002/esp.1855.
- 322 Whitfield, D., Baynes, E.R.C., Hodge, R.A., Rice, S.P., and Yager, E.M., 2025, The Influence of
323 Gravel-Bed Structure on Grain Mobility Thresholds: Comparison of Force-Balance
324 Approaches: Journal of Geophysical Research: Earth Surface, v. 130, p. e2025JF008333,
325 doi:10.1029/2025JF008333.
- 326 Wong, M., and Parker, G., 2006, Reanalysis and Correction of Bed-Load Relation of Meyer-
327 Peter and Müller Using Their Own Database: Journal of Hydraulic Engineering, v. 132,
328 p. 1159–1168, doi:10.1061/(asce)0733-9429(2006)132:11(1159).
- 329 Yager, E.M., Schmeeckle, M.W., and Badoux, A., 2018, Resistance Is Not Futile: Grain
330 Resistance Controls on Observed Critical Shields Stress Variations: Journal of
331 Geophysical Research: Earth Surface, v. 123, p. 3308–3322,
332 doi:<https://doi.org/10.1029/2018JF004817>.
- 333 Yager, E.M., Turowski, J.M., Rickenmann, D., and McArdell, B.W., 2012, Sediment supply,
334 grain protrusion, and bedload transport in mountain streams: Geophysical Research
335 Letters, v. 39.

336

337

338 FIGURE CAPTIONS

339 **Figure 1.** A) sediment transport rating curves; B) Estimates of τ_{ref}^* with channel slope; error

340 bars represent the 75% confidence interval.

341 **Figure 2.** Normalized sediment flux, q_{s_n} , with conditioning time for each experimental slope and
342 data from Masteller and Finnegan (2017) with best-fit power laws.

343 **Figure 3.** Riverbed strengthening exponent, ζ , as a function of slope. Error bars denote ± 1
344 standard deviation uncertainty associated with the power-law fits used to estimate ζ .

345

346 ¹Supplemental Material. [Expanded methods description and experimental data](#). Please visit
347 <https://doi.org/10.1130/XXXX> to access the supplemental material, and contact
348 editing@geosociety.org with any questions.

Slope-dependent riverbed strengthening and the evolution of the threshold for motion in gravel-bed rivers

Robert Kostynick¹, Julia Prata¹, Jesse Bower², Jedidiah Dale¹, and Claire Masteller¹

¹*Earth, Environmental, and Planetary Sciences, Washington University in St. Louis, St. Louis, MO, USA*

²*Department of Civil & Environmental Engineering, Utah State University, Logan, UT, USA*

S1. Sediment transport rating curves, estimation of reference Shields stress, and hydraulic scaling

At each experimental slope, a sediment transport rating curve was constructed for a range of flow depths. Flow depths were adjusted between each experimental run by varying the frequency of an adjustable pump drive with a frequency precision of 0.1 Hz. Each rating curve run had a duration of 3 minutes, during which sediment transport out of the flume was caught in a downstream basket. Flow depths were measured at one upstream, central, and downstream position along the flume using a ruler. At the end of each run, sediment transported out of the flume was weighed, providing a total sediment flux over each 3-minute trial.

Flow depth at a given pump frequency decreases with increasing slope for a given transport condition, such that the range of stable flow depths that could be explored became progressively narrower at steeper slopes. Because of the multiplicative effect of slope on shear stress, this compression in flow depth still produced a wider range of shear stresses even over a smaller range of flow depths and associated pump frequencies. At the steepest slopes, experiments were additionally limited by episodic bed failure, which constrained the number of runs that could be conducted. As a result, rating curves at higher slopes are based on a more limited range of flow conditions and therefore carry greater uncertainty.

To convert average flow depths for each experiment to dimensionless Shields stress, τ^* , we used

$$\tau^* = \frac{\rho g R S}{(\rho_s - \rho) g D_{50}} \quad (1).$$

Where ρ and ρ_s are water and sediment density, respectively, with units kg/m³, g is acceleration due to gravity (m/s²), R is the hydraulic radius (m), S is channel slope (m/m), and D_{50} is median grain size (m). Slope and hydraulic radius vary for each

experimental run (See Supplementary Dataset), all other parameters are held constant (Table S1).

Table S1. Parameter values for Shields stress calculation

Parameter	Value
water density, ρ	1000 kg/m ³
sediment density, ρ_s	2650 kg/m ³
gravity, g	9.81 m/s ²
median grain size, D_{50}	0.074 m

Following conversion from flow depth to Shields stress, we convert total flux to dimensionless transport rate, defined as

$$q_s^* = \frac{q_s}{\sqrt{\frac{\rho_s - \rho}{\rho} g D_{50}^3}} \quad (2),$$

where q_s is the dimensional flux rate (kg/m/s), calculated as the total bedload flux divided by the run time and the flume width. To estimate τ_{ref}^* , we fit a power law to each slope-specific rating curve. We then use these best-fit power law relationships to estimate τ_{ref}^* at a reference transport rate $q_s^* = 0.08$. We selected this reference transport rate to ensure that two data points from each rating curve experiment fell below this reference rate. We note that following this procedure, the selection of a lower reference transport rate would compress the range of τ_{ref}^* , but would not meaningfully change the form or goodness-of-fit between τ_{ref}^* and slope.

We note that we completed this procedure at 5 slopes, $S = 5, 10, 25, 50,$ and 70 mm/m. However, we did not conduct conditioning experiments at $S = 10$ mm/m, instead incorporating previous experiments from Masteller and Finnegan (2017). Nevertheless, the additional rating curve helps to inform the relationship between slope and τ_{ref}^* , as well as the hydraulic scaling used in our low flow conditioning experiments, so we opt to include it here.

Based on τ_{ref}^* estimates, flow depths and pump frequencies were selected to target approximately $0.75\tau_{ref}^*$ and $1.2\tau_{ref}^*$, while accounting for uncertainty in the rating-curve estimates of τ_{ref}^* . Some trial and error was required to ensure that the experiments captured conditioning and sediment-transporting flow conditions and prevent bed failure at steep slopes. Consistent with this design, little to no sediment transport was observed during conditioning phases.

S2. Low flow conditioning experiments

Across all experiments, sediment flux decreases systematically with increasing conditioning time. Three of the four experimental slopes ($S = 0.025$ – 0.070 m/m) occupy

a similar range of sediment flux values and exhibit comparable declines in flux with conditioning time. In contrast, the lowest slope experiment ($S = 0.005$ m/m) shows systematically lower flux values, which likely reflects uncertainty in the transport flow associated with the rating-curve-derived hydraulic scaling. Data from Masteller and Finnegan (2017) plot above the new experimental data. This offset is not unexpected, as those experiments were conducted at a different facility and slope effects were not explicitly accounted for when estimating the hydraulic scaling between conditioning and transport phases. These offsets are captured by the coefficients of the best-fit power laws, whereas the riverbed strengthening exponents, which quantify the rate of flux reduction with conditioning time, vary systematically with slope.

To facilitate comparison across slopes and with previous experiments from Masteller and Finnegan (2017) ($S = 8$ mm/m), q_s was normalized using the data-derived regression for each experiment. Specifically, flux values were rescaled by the flux predicted by the best-fit regression at $t = 1$, effectively normalizing by the coefficient of each regression.

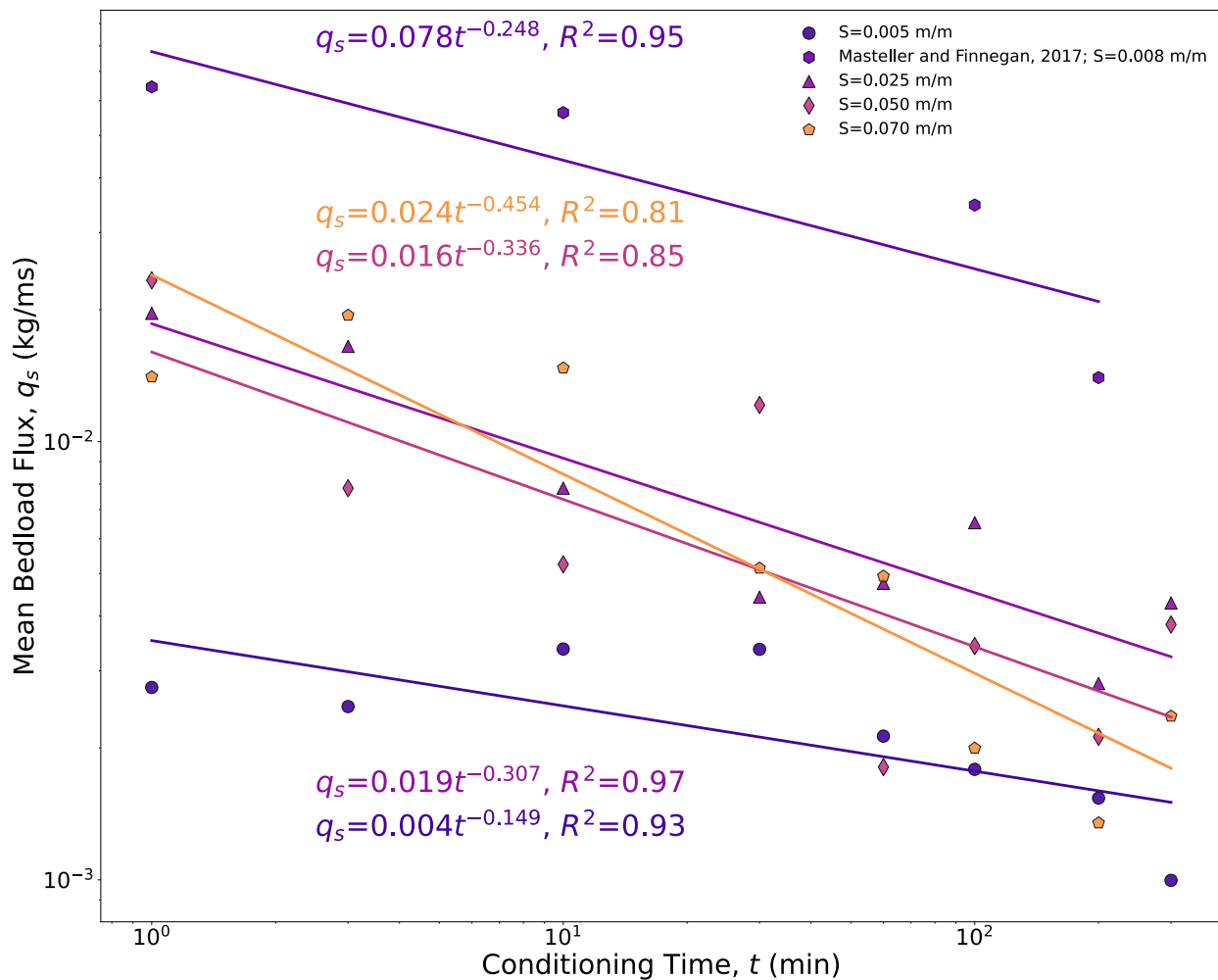


Figure S1. Mean bedload flux measurements as a function of conditioning time with best-fit power laws and goodness-of-fit metrics.

Summary of Supporting Dataset

We provide the experimental dataset supporting this contribution as a .xls file. In the provided file we provide the experimental data from rating curve construction, estimates of τ_{ref}^* , antecedent low flow experimental data, and ζ values.

Table 1. Rating Curve Data.

Slope, S (m/m)	Average Flow Depth, h (m)	Hydraulic Radius, R (m)	Shield Stress , Tau*	Run Time (s)	Total Sediment Flux, Qs_total (kg)	Sediment Flux, qs (kg/m/s)	Dimensionless sediment flux, qs*
0.005	0.023	0.020	0.008	180	4.200E-04	5.819E-06	2.272E-03
0.005	0.035	0.030	0.012	180	8.530E-03	1.182E-04	4.614E-02
0.005	0.043	0.035	0.014	180	1.512E-01	2.095E-03	8.181E-01
0.005	0.051	0.040	0.017	180	2.441E-01	3.382E-03	1.321E+00
0.005	0.059	0.045	0.019	180	2.612E-01	3.618E-03	1.413E+00
0.005	0.066	0.050	0.020	180	6.682E-01	9.257E-03	3.614E+00
0.005	0.075	0.055	0.022	180	1.268E+00	1.757E-02	6.859E+00
0.005	0.073	0.054	0.022	180	9.157E-01	1.269E-02	4.954E+00
0.005	0.079	0.056	0.023	180	1.997E+00	2.766E-02	1.080E+01
0.01	0.015	0.014	0.011	180	9.700E-04	1.344E-05	5.247E-03
0.01	0.024	0.021	0.017	180	1.459E-02	2.021E-04	7.892E-02
0.01	0.035	0.030	0.025	180	8.056E-02	1.116E-03	4.358E-01
0.01	0.044	0.036	0.030	180	2.160E-01	2.993E-03	1.169E+00
0.01	0.056	0.044	0.036	180	5.242E-01	7.263E-03	2.836E+00
0.01	0.059	0.045	0.037	180	1.026E+00	1.421E-02	5.548E+00
0.025	0.006	0.006	0.013	180	6.000E-05	8.313E-07	1.257E-02
0.025	0.015	0.014	0.029	180	5.470E-03	7.578E-05	2.857E-02
0.025	0.018	0.017	0.034	180	2.440E-02	3.380E-04	3.439E-02
0.025	0.023	0.020	0.042	180	4.256E-02	5.896E-04	4.170E-02
0.025	0.028	0.025	0.050	180	1.020E-01	1.412E-03	5.030E-02
0.025	0.029	0.026	0.052	180	1.215E-01	1.683E-03	5.239E-02
0.025	0.025	0.022	0.046	180	4.357E-01	6.036E-03	4.551E-02
0.025	0.028	0.025	0.051	180	3.068E-01	4.250E-03	5.083E-02
0.025	0.032	0.028	0.057	180	4.154E-01	5.755E-03	5.650E-02
0.025	0.034	0.029	0.060	180	2.112E-01	2.926E-03	6.002E-02
0.025	0.032	0.028	0.057	180	1.813E-01	2.511E-03	5.650E-02
0.025	0.036	0.030	0.062	180	4.222E-01	5.849E-03	6.200E-02
0.025	0.033	0.028	0.058	180	9.341E-01	1.294E-02	5.751E-02
0.025	0.035	0.030	0.062	180	8.874E-01	1.229E-02	6.151E-02
0.025	0.040	0.034	0.069	180	3.537E+00	4.901E-02	6.875E-02
0.05	0.005	0.005	0.021	180	7.000E-05	9.698E-07	3.787E-04
0.05	0.011	0.011	0.044	180	6.540E-03	9.061E-05	3.538E-02
0.05	0.013	0.012	0.050	180	9.263E-02	1.283E-03	5.011E-01
0.05	0.018	0.017	0.068	180	2.561E-01	3.548E-03	1.385E+00

0.05	0.021	0.019	0.077	180	1.488E-01	2.061E-03	8.047E-01
0.05	0.021	0.019	0.079	180	4.693E-01	6.502E-03	2.539E+00
0.07	0.005	0.005	0.028	180	8.000E-05	1.108E-06	4.328E-04
0.07	0.009	0.009	0.049	180	2.150E-03	2.979E-05	1.163E-02
0.07	0.018	0.017	0.095	180	1.881E-01	2.606E-03	1.018E+00
0.07	0.020	0.018	0.106	180	1.398E-01	1.937E-03	7.564E-01
0.07	0.019	0.017	0.099	180	1.139E+00	1.578E-02	6.160E+00

Table 2. Reference Shields Stress Estimates

Slope	Reference Shields Stress
0.005	0.012
0.01	0.018
0.025	0.032
0.05	0.046
0.07	0.063

Table 3. Low Flow Conditioning Experimental Data

Slope	Conditioning Time	Average bedload flux, kg/m/s	Normalized Bedload Flux	
0.005	1	0.004	0.966	
0.005	3	0.002	0.570	
0.005	10	0.003	0.771	
0.005	30	0.003	0.770	
0.005	60	0.002	0.488	
0.005	100	0.002	0.410	
0.005	200	0.002	0.352	
0.005	300	0.001	0.229	
0.008	1	0.065	0.831	Masteller and Finnegan, 2017
0.008	10	0.056	0.726	Masteller and Finnegan, 2017
0.008	100	0.035	0.447	Masteller and Finnegan, 2017
0.008	200	0.014	0.180	Masteller and Finnegan, 2017
0.025	1	0.020	1.056	
0.025	3	0.017	0.888	
0.025	10	0.008	0.422	
0.025	30	0.004	0.238	
0.025	60	0.005	0.256	
0.025	100	0.007	0.352	
0.025	200	0.003	0.151	
0.025	300	0.004	0.231	
0.050	1	0.023	1.458	
0.050	3	0.008	0.489	
0.050	10	0.005	0.328	
0.050	30	0.012	0.757	
0.050	60	0.002	0.113	
0.050	100	0.003	0.213	
0.050	200	0.002	0.132	
0.050	300	0.004	0.239	
0.070	1	0.014	0.585	
0.070	3	0.019	0.809	
0.070	10	0.015	0.613	
0.070	30	0.005	0.214	
0.070	60	0.005	0.205	
0.070	100	0.002	0.083	
0.070	200	0.001	0.056	
0.070	300	0.002	0.098	

Table 4. Strengthening Exponents

Slope	Strengthening exponent
0.005	0.198
0.008	0.248
0.025	0.307
0.05	0.336
0.07	0.454

